Smart Materials and Structures

PAPER

Multilayer laminated piezoelectric bending actuators: design and manufacturing for optimum power density and efficiency

To cite this article: Noah T Jafferis *et al* 2016 *Smart Mater. Struct.* **25** 055033

View the article online for updates and enhancements.

You may also like

- Apparent and steady-state etch rates in thin film etching and under-etching of microstructures: I. Modelling
Gregory Van Barel, Luc Mertens, Ward De Ceuninck et al.
- Compact model for PZT ferroelectric capacitors with voltage dependent switching behavior
Chien-Wei Wang, Hansol Ku, Cheng Yan Chiu et al.
- ZnO thin film piezoelectric micromachined microphone with symmetric composite vibrating diaphragm
Junhong Li, Chenghao Wang, Wei Ren et al.

This content was downloaded from IP address 128.103.24.19 on 24/04/2022 at 13:12

IOP Publishing Smart Materials and Structures
Smart Mater. Struct. 25 (2016) 055033 (13pp) doi:10.1088/0964-1726/25/5/055033

Multilayer laminated piezoelectric bending actuators: design and manufacturing for optimum power density and efficiency

Noah T Jafferis[1], Mario Lok[1], Nastasia Winey[2], Gu-Yeon Wei[1] and Robert J Wood[1]

[1] John A Paulson School of Engineering and Applied Sciences and the Wyss Institute for Biologically Inspired Engineering, Harvard University, Cambridge, MA 02138, USA
[2] Johns Hopkins University, Baltimore, MD 21218, USA

E-mail: njafferis@seas.harvard.edu, mlok@seas.harvard.edu, nwiney1@jhu.edu, gywei@g.harvard.edu and rjwood@eecs.harvard.edu

Received 9 December 2015
Accepted for publication 21 March 2016
Published 13 April 2016

Abstract

In previous work we presented design and manufacturing rules for optimizing the energy density of piezoelectric bimorph actuators through the use of laser-induced melting, insulating edge coating, and features for rigid ground attachments to maximize force output, as well as a pre-stacked technique to enable mass customization. Here we adapt these techniques to bending actuators with four active layers, which utilize thinner material layers. This allows the use of lower operating voltages, which is important for overall power usage optimization, as typical small-scale power supplies are low-voltage and the efficiency of boost-converter and drive circuitry increases with decreasing output voltage. We show that this optimization results in a 24%–47% reduction in the weight of the required power supply (depending on the type of drive circuit used). We also present scaling arguments to determine when multi-layer actuator are preferable to thinner actuators, and show that our techniques are capable of scaling down to sub-mg weight actuators.

Keywords: actuators, multi-layer, efficiency, sub-mg, piezoelectric, power electronics, power density

(Some figures may appear in colour only in the online journal)

1. Introduction

At small scales (approximately centimeter-scale and below), piezoelectric actuators (see [1] for previous work on optimizing the energy density of PZT bimorph actuators) are an attractive option for driving high-frequency oscillatory devices due to their favorable scaling. In contrast, motors become less efficient as their size is reduced, in part due to the ℓ^4 scaling of the electromagnetic force [2]. However, we are actually interested in small-scale devices that have high performance from a system perspective, which means that we must include small-scale power and drive electronics in our analysis. In this context, one of the downsides of piezoelectric actuators is the mismatch between the hundreds of volts typically required for such actuators and the 3–4 V provided by small-scale power supplies such as LiPo batteries. This requires boost converter and drive circuitry, which can have relatively low combined efficiency (defined as the $0.5CV^2f$ divided by the input power) when providing such high voltage at small scales (~30%–60% for a 300 V output, see [3] and below). To alleviate this issue and obtain maximal system efficiency, it is desirable to use piezoelectric layers that are as thin as possible to minimize voltage while maintaining the desired electric field in order to maintain maximal energy density. To achieve this without changing the mechanical properties or shape of the actuator (see section 5 for a discussion on the shape tradeoff), multiple layers of piezoelectric materials must be used. While this can be addressed by using

 © 2016 IOP Publishing Ltd Printed in the UK

thin-films for micro-scale devices, mm–cm scale devices typically require total actuator thicknesses of hundreds of microns in order to provide sufficient force. This means that bulk piezoelectric sheets are used, which are limited in how thin they can be fabricated due to their brittle nature.

Previous work on multilayer piezoelectric bending actuators has mostly focused on thin-film piezoelectrics [4, 5], which are appropriate for micro-scale devices but typically do not have sufficient output power for mm–cm scale devices. Additionally, bulk piezoelectrics generally have higher piezoelectric coefficients and are not limited to mm-size crack-free areas [6, 7]. There have been several reports of multilayer bending actuators made with bulk materials, such as [8]. Screen-printing is another method, which can produce actuators between these scales [9]. Further, while thin-film piezoelectric bending actuators have been fabricated with lateral dimensions down to tens of microns [10], the smallest actuators fabricated from bulk sheets are in the range of hundreds of microns to millimeters (e.g. [11], which utilizes interdigitated electrodes on beams of bulk PZT down to 1 mm by 380 μm by 127 μm). Boost-converter and drive circuits at an appropriate scale (below 100 mg) for our applications have also been developed [3].

2. Advantages of multilayer actuators—power considerations

In most applications, piezoelectric actuators draw energy from a low-voltage source, such as a 3–4 V Lithium Polymer battery, but require drive signals in the range of a hundreds of volts because high electric fields maximize the actuators' output power density and thus minimize their weight. In these applications, a power electronics circuit typically serves as an intermediate unit between the power source and the actuator. One of the advantages of multilayer actuators is that they reduce the required drive voltages for a given output power requirement. With a reduced drive voltage magnitude, the power electronics can deliver energy from the power source more efficiently. To illustrate this effect in detail, here we analyze two power electronics designs that were previously shown to be feasible at small size scales (less than 100 mg total).

Both power electronics topologies of interest, shown in figures 1(a) and (b), consist of two stages. The first stage is a boost converter that draws energy from the power source (assumed to be 3.7 V, which is typical of LiPo batteries, for all of the plots shown in this work), and outputs a constant high voltage VDDH (in the range of 100–300 V). The second stage is a driver circuit that draws energy from VDDH and generates the desired sinusoidal drive signal (which varies between 0 V and VDDH) for the actuator. Given that most of the energy stored in the capacitive structure of the actuator is not dissipated, when generating the sinusoidal drive signal, the driver circuit sources energy into the actuator in one half-cycle and extracts energy from the actuator in the other half-cycle. The total power consumed from the battery is a combination of the power dissipated by losses in the boost converter and the power dissipated by the driver circuit in the process of delivering and withdrawing energy. Reducing the drive voltage (while maintaining fixed output power) can thus have an impact on both the boost converter and the driver circuit efficiencies.

To understand how a reduced output voltage impacts the boost converter efficiency, we can look at its detailed implementation (tapped-inductor topology) shown in figure 1(c). The parasitic resistance and capacitance are also shown in the schematic. In each energy conversion cycle, the switch is turned on to charge the primary winding of the coupling inductor. When the switch turns off, the energy stored in the coupling-inductor is discharged by current flowing from the secondary winding to the output VDDH via the output diode. At the end of the conversion cycle, a finite amount of energy is drawn from the output VDDH to charge the parasitic capacitance of the output diode back to (VDDH $-$ V_{BAT}). The boost converter dissipates energy in the form of conduction loss through the equivalent resistance of the primary winding, the secondary winding, the transistor switch and the output diode, and suffers switching losses due to energy spent to turn on and off the transistor switch in each conversion cycle. In addition, even though energy drawn from the output to charge the parasitic capacitance of the output diode is not dissipated, it simultaneously reduces the input energy and output energy per conversion cycle, effectively lowering the efficiency. Among these parasitic effects, the impact of the secondary winding resistance and the parasitic capacitance of the output diode reduces as the output voltage decreases, while the other effects have a much smaller dependence on the output voltage. Thus, the boost converter efficiency improves monotonically as the output voltage decreases at fixed output power. Figure 2(a) shows the measured efficiency of such a converter with light-weight power semiconductors and a custom hand-wound inductor.

Two general types of drive topology are now considered, with the following tradeoff: type A (figure 1(d)) uses an inductor to allow energy recovery when driving a capacitive load, and is thus more efficient but also heavier (100 mg versus 50–60 mg) than type B (figure 1(e)), which does not use this inductor, but can employ other power saving techniques. The actuator can also have two different configurations (figure 1(f)). For the type A driver topology, the actuator is configured in simultaneous drive topology, where the capacitive loads are series-connected.

The type A driver topology, a switching amplifier [3], consists of a half bridge driver with an output inductor. In each conversion cycle, the output inductor provides intermediate energy storage, allowing bidirectional efficient energy transfer between the high voltage supply VDDH and the actuator capacitive loads. However, as the transistor switch turns on and off, the switching loss per energy conversion cycle, contributed by the parasitic output capacitance C_{DS} of the switch (figure 1(d)), becomes a bottle neck for the driver circuit to deliver or recover energy efficiently. The loss contribution of C_{SW} in each conversion cycle depends on the instantaneous voltage on the actuator, but on average it scales with $0.5C_{\mathrm{SW}}V^2$, where V is the peak-to-peak drive voltage

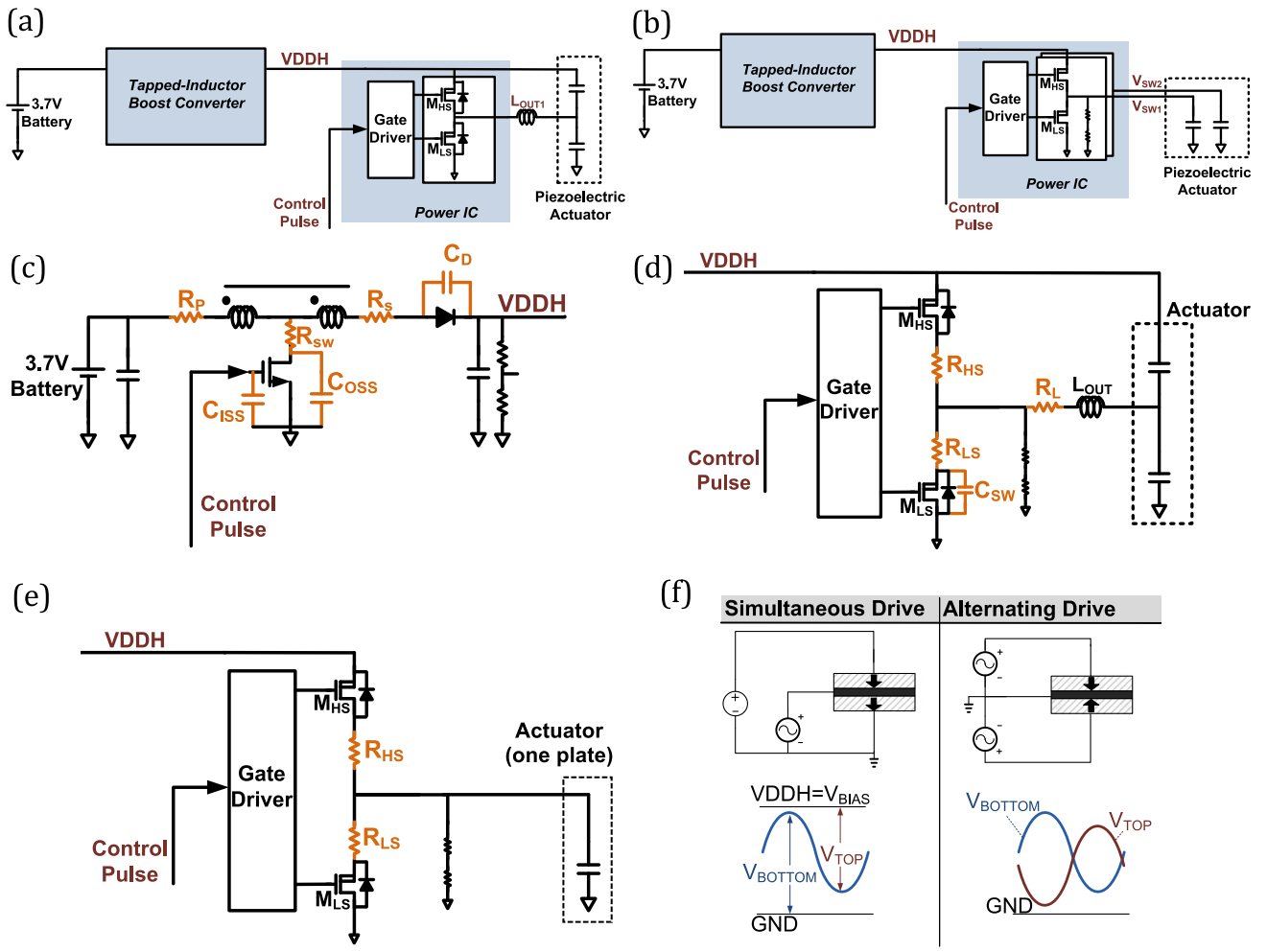

Figure 1. (a) The type A topology consists of a tapped-inductor boost converter with a switching amplifier driver stage. (b) The type B topology consists of a tapped-inductor boost converter and linear drivers. (c) Detailed diagram showing the parasitic elements that contribute to energy loss in the tapped-inductor boost converter. (d) and (e) show the parasitic elements that contribute to energy loss in the type A and type B driver topologies, respectively. (f) Two actuator configurations are simultaneous drive (used in the type A topology), where the piezoelectric layers are series-connected, and alternating drive (used in the type B topology), where the piezoelectric layers are parallel-connected.

amplitude. Therefore, the drive voltage magnitude reduction achieved through employment of multilayer actuators translates into quadratic reduction in switching losses. In addition, a reduction in the drive voltage magnitude enables designers to use transistors with lower voltage rating for the driver circuits. As the parasitic capacitance C_{SW} has a steep dependency on the voltage rating of the transistor, using lower voltage transistors in the driver circuit can further lessen the switching loss by reducing C_{SW}. For example, compared to the parasitic capacitance C_{SW} of power transistors in a 300 V process, such as the ones used in [12, 13], the parasitic capacitance C_{SW} in a 200 V process would be smaller by a factor of eight.

The type B driver topology, proposed in [12], configured the actuator in alternating drive configuration. It employs two variations—'linear' and 'envelope tracking'. In both variations, the driver linearly charges and discharges the capacitive load, and does not fully discharge C_{SW} in each conversion cycle (figure 1(e)). Thus, the power consumption of the driver in this topology is expected to be independent of the voltage (for fixed output power), but we still consider this topology in our analysis since the boost converter's efficiency will still be increased.

To analyze the performance of the above boost and driver circuits with the multi-layers actuators, we developed a power model capturing the power consumption for the boost converter and drivers of both types. The model estimates the total power consumption of the power electronics while sweeping actuator drive voltage amplitude and keeping total power constant. The power numbers predicted by the model are validated against measurement data of the physical implementation described in [12, 13]. The power model gives the total power consumption of the power electronics based on both type A and type B driver implemented in a 300 V process. The result of the type A driver is denoted as 'SW AMP 1' while the two variations of type B are denoted as 'linear' and 'EVT'. In addition, the model also predicts the total

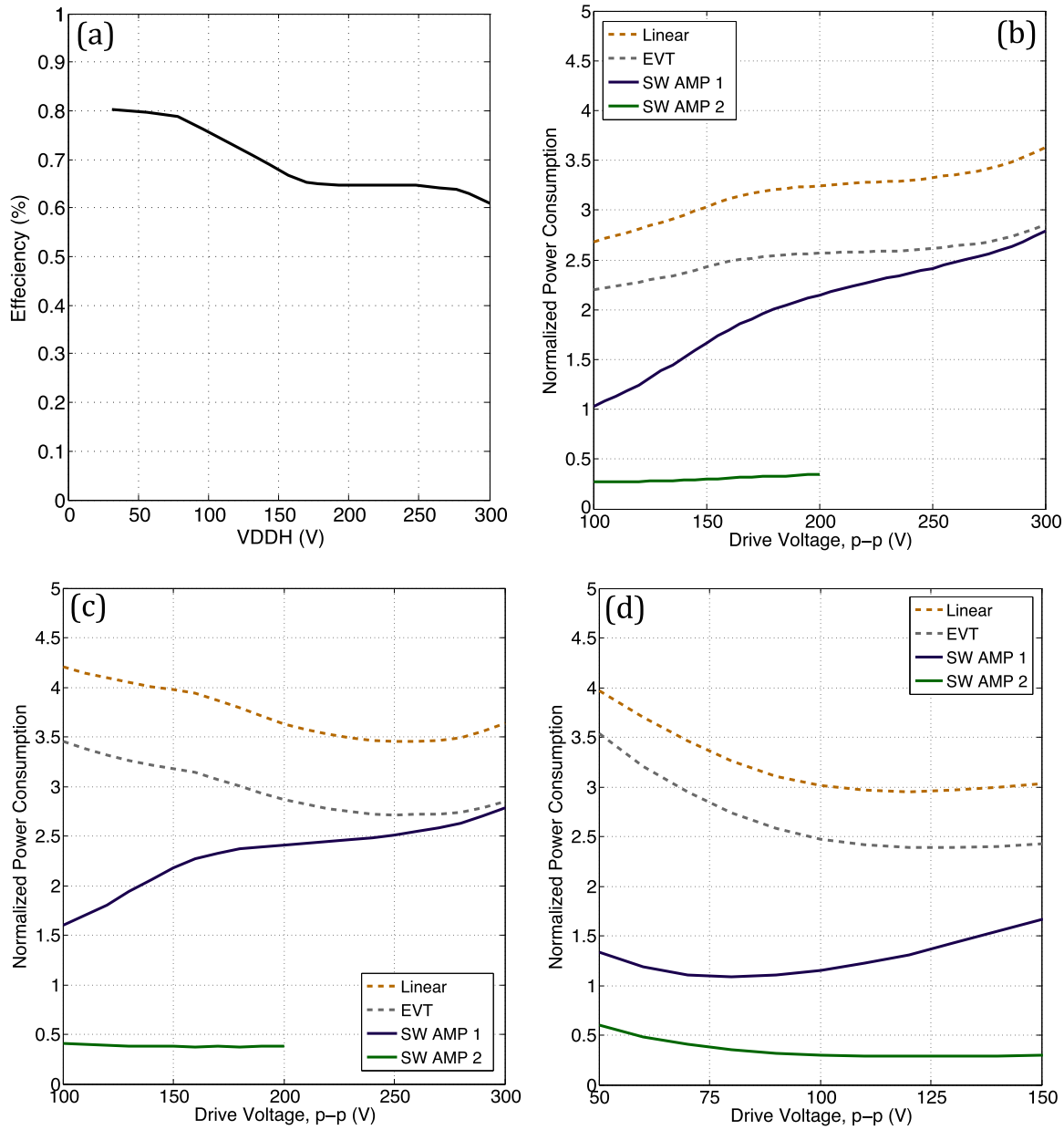

Figure 2. (a) Efficiency of the boost converter as a function of output voltage. (b) The required power-supply power (normalized to $0.5CV^2f$) for constant $0.5CV^2f = 54$ mW for several circuit topologies as a function of driving voltage. For this plot, f is 120 Hz and C is 10 nF $\times$ $(300\ \mathrm{V/V})^2$. (c) Same as (b), except that the mechanical output power of the actuator ($d_{\mathrm{f,\ 1\text{-}way}} \times F_{\mathrm{b,\ 1\text{-}way}} \times f = 12.7$ mW) is kept fixed instead of $0.5CV^2f$ (the normalization is still to the nominal value of $0.5CV^2f$). This thus takes into account nonlinearities in the actuator's mechanical output power and electrical input power. (d) Equivalent to (c) except for an 'ideal' four-layer actuator (i.e. with the same performance as the two-layer actuator, just with each layer split in two).

power consumption of a type A driver implementation in a 200 V process. We denote this scenario as 'SW AMP 2'.

To understand the power savings provided by employing multi-layers actuators, we first consider what happens when driving an ideal capacitive load. The output electrical power, P_{L}, of the drive stage is defined to be $0.5CV^2f$, where C is the capacitance of the load capacitor, V is the peak-to-peak value of the voltage applied to the capacitor (for this paper, this is always set to VDDH), and f is the drive frequency. We further define the relative input power, p_{r}, as the input power, P_{in}, (from the power supply) divided by P_{L}. Figure 2(b) plots p_{r} for fixed P_{L} as a function of voltage for the various circuit topologies described above (i.e. since P_{L} is kept fixed as V is varied, a lower voltage corresponds to a larger load capacitance). As can be seen, these circuits are more efficient at lower voltages. It is important to note, however, that the PZT actuators have several nonlinearities that need to be included in order to determine the overall efficiencies. One of these effects is variation of the dielectric constant of the PZT with electric field (described in [3] and shown in figure 5(d)), and the other is the field-dependent nonlinearity of the piezoelectric coefficient [1]. Figure 2(c) shows what happens when we plot p_{r} for fixed mechanical output power of the actuator (which means that at lower voltages, the actuator is larger)—

since the dielectric constant of the PZT increases as the voltage drops from 300 to 100 V (for 135 μm PZT), and the actuator's efficiency (mechanical output power divided by electrical input power) is lower at low voltages, the required input power is no longer reduced at lower voltages for the type B circuits and does not drop as quickly for the type A circuits. However, since the efficiency of the actuator is dependent on the field, while the boost/drive circuit efficiency depends on the voltage, we still expect a benefit from switching to multiple layers of PZT. Bulk PZT sheets are commercially available with thicknesses down to 50–60 μm —this is about half of the 135 μm sheets used in our previous work (e.g. [1, 14, 15]), so in this paper our goal is actuators with four PZT layers which should roughly halve the operating voltages (and double the current). The result is shown in figure 2(d), which plots p_r for an 'ideal' four-layer actuator (note that, in this work, we refer to only the number of active layers in the device; hence a 'four-layer' actuator means four PZT layers plus inactive adhesive layers)—that is, if the efficiency of such an actuator is identical to the standard two-layers ones at the same field, but voltage is halved and the capacitance quadrupled (i.e. each layer is split into two layers). Based on these plots we expect that switching to four layers of thinner PZT will result in a power savings of 15%–40% (depending on which drive circuit is used), even without including the further power reduction expected from the 'SW AMP 2' 200 V process.

To characterize the expected improvement from a system perspective, we need to include the weight of the actuator and the weight of the boost and drive circuit. This depends on the battery power density and the mass of the actuator being driven relative to the mass of the circuitry, but for the purposes of this paper, we will take the battery power density to be 1 mW mg^{-1}, which is within the specifications for small LiPo batteries (for example, Power Stream's 400 mg PGEB201212 battery, which is rated at 10 mAH, 4.2 V, and 10–15 C discharge, and can provide 400 mW at 3.6 V, 11 C). Further, we take the actuator size to be that of two Robobee actuators [14], which together have a nominal capacitance of 10 nF for both plates and a mechanical output power of 12.7 mW at 300 V p–p. The mechanical power is defined here as the maximum deflection in one direction times the maximum force in one direction times the frequency, or $d_{\text{f,1-way}} \times F_{\text{b,1-way}} \times f$. This metric is used because it is analogous to the $0.5CV^2f$ expression used for the electrical power. That is, when the actuator bends fully in one direction, the strain potential energy is $0.5\,\text{K}(d_{\text{f,1-way}})^2$, where K is the stiffness of the actuator. In each bending cycle, the actuator bends first in one direction, and then in the other direction, and to first order $d_{\text{f,1-way}} = F_{\text{b,1-way}}/K$, resulting in an available strain energy of $d_{\text{f,1-way}} \times F_{\text{b,1-way}}$ per cycle. Note that the actual power output can be lower or higher than this value, depending on whether or not the system is in resonance and on the details of the load attached to the actuator. We can then use the measurements on the standard two-layer actuators [1] to plot the mass of the actuator required to achieve this fixed mechanical output power as a function of the applied voltage, and we also plot the expected actuator mass for an 'ideal' four-layer actuator with identical dimensions (i.e. just splitting each PZT plate into two layers), which gives the same mass at half the voltage. Similarly, we can use the boost-converter and drive circuit efficiencies discussed above to plot the mass of the required battery as a function of voltage, both for the standard two-layer actuators and the 'ideal' four-layer ones. Since each different boost/drive circuit results in a different battery mass, only two of the drive topologies ('linear' and 'SW AMP 1') are used in this plot for simplicity (one of type A, one of type B). The mass of the boost/drive circuit, along with the total mass of all three of these elements is also shown. All of these plots are shown in figure 3, and demonstrate that from a system perspective, there is an 'optimal' operating voltage that minimizes the total mass of the actuator and power supply/circuitry. Further, the reduction in operating voltage enabled by the 'ideal' four-layer structure would result in a total weight savings of about 11%–20% for the given circuit topologies, actuator size and battery power density. A six-layer structure would reduce this further, but due to the added fabrication complexity and limited availability of thinner material, we focus here on four-layer devices. Further, there are diminishing returns as the number of layers is increased—for example, once the voltage is below 200 V the prediction for the 'SW AMP 2' scenario indicates that the power consumption could be less than a third of $0.5CV^2f$, which is already in the range in which the actual power consumption of the actuator (i.e. the mean value of the applied voltage times the current) can no longer be neglected.

3. Fabrication process

The four-layer actuators are fabricated as follows: first, two sheets of 60 μm PZT (5H, 3203HD) are bonded together with a 12 μm conductive adhesive film (ESP8660) in a heat press (at a temperature of 180 °C and pressure of about 15 psi for two hours). Rectangles are then cut from this laminate using a diode-pulsed solid-state laser (Photonics Industries DC150H-355, a Nd:YVO4 laser with 355 nm wavelength and 10 μm spot size) set to 20 kHz, 20 cm s^{-1}, and 0.24 W average power—these rectangles are used in place of the rectangles of 135 μm PZT used in the standard two-layer 'pre-stack' method described in [1], and the remainder of the lamination steps are identical to those used in the 'pre-stack' process [1] (with one slight modification, which is recommended for the standard two-layer process as well: in the 2nd cure cycle, a 25 μm sheet of FEP and a layer of Pacopad (a crushable material, Pacothane Technologies, Wincester, MA) are placed on top of the copper/CF layers to create a more uniform pressure profile over the step of the bridges—see figure 4(a)). Most of the laser cutting steps are also identical to the 'pre-stack' process, with two added laser-etching steps to make contact with the conductive adhesive films: (1) a hole is rastered through the CF bridge and the outer PZT layers. To avoid rastering through the conductive adhesive, which is only 12 μm thick, it is necessary for the PZT to be etched uniformly. However, the standard etch pattern (a series of parallel lines at 0° and 90°) results in deeper etching around

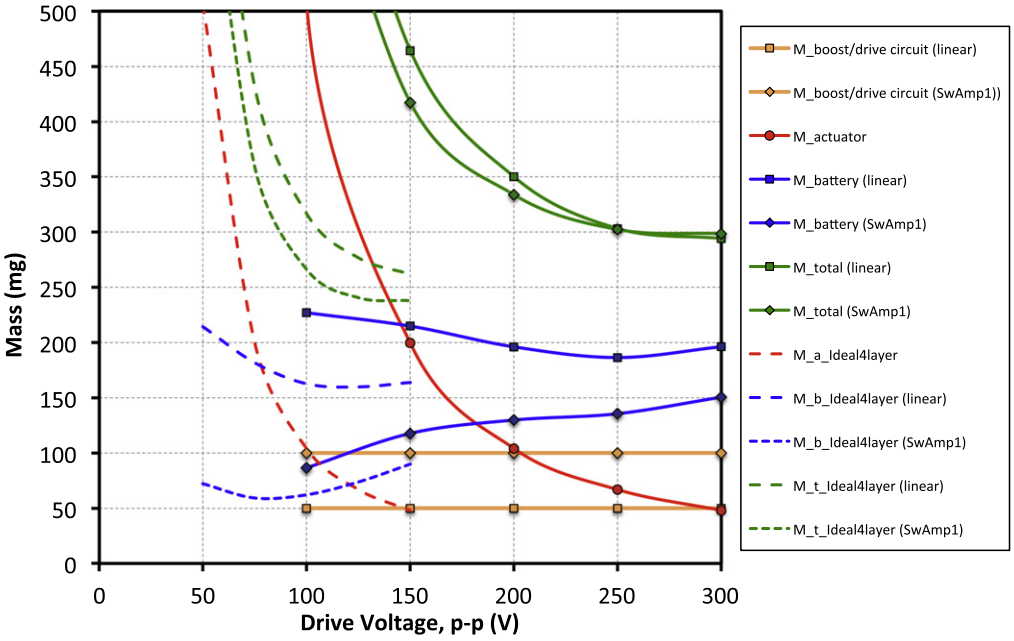

Figure 3. Required masses of an actuator (red), battery (blue), boost-converter and drive circuit (orange), and their total sum (green) plotted versus voltage for a fixed output power of $d_{\text{f, 1-way}} \times F_{\text{b, 1-way}} \times f = 12.7$ mW. Solid lines are for two-layer actuators, while dashed lines are for an 'ideal' four-layer actuator (i.e. with the same performance as the two-layer actuators, just at half the voltage and four times the capacitance).

the edges, which cuts though the conductive adhesive. This is because the laser must decelerate/accelerate at the ends/beginnings of each line, and is thus moving more slowly near the edges of the rastered hole. To solve this, a different raster pattern was designed which has constant curvature nearly everywhere (figure 4(d)), resulting in a more uniform cutting speed and etch. (2) The part of the CF/copper layer that abuts the hole through the PZT must be separated from the rest of the CF/copper (which is electrically connected to the top surface of the PZT)—this is achieved with a raster step that etches through the CF and slightly into the PZT to ensure that the top metal coating is removed. The copper is etched in the same step that patterns the copper/CF over the alumina base. Note that when the CF is rastered over the alumina–PZT interface, it is possible that CF debris could lodge in any tiny gap between the alumina and PZT, resulting in shorting. To avoid this possibility, a small amount of cyanoacrylate (CA) glue was applied to this seam before the bridges were bonded on. Sufficient post-etch cleaning might eliminate the need for this step.

The resulting actuators (figures 4(b) and (c)) have a nearly identical form factor to the two-layer versions (3.5 mm base width, 0.5 mm tip width, 3.2 mm long extension, and a total thickness of ~320 μm), allowing them to be used as drop-in replacements. The only differences are that the four-layer actuators consist of four 60 μm PZT layers, two 12 μm conductive adhesive layers, and one 50–55 μm CF layer, while the two-layer actuators consisted of two 135 μm PZT layers and one 50–55 μm CF layer. The weight of the four-layer actuators is also slightly less—49 mg instead of 51 mg (these actuators had a slightly larger alumina base than the 42 mg actuators reported in [1]).

4. Results

To characterize the four-layer actuators, blocked-force and free deflection measurements are performed, and the results are compared with those of the standard two-layer actuators from [1], as shown in figures 5(a) and (b). Figure 5(c) shows the mechanical energy output of the devices (defined here as $d_{\text{f,1-way}} \times F_{\text{b,1-way}}$). While the four-layer actuators function out to similar forces and deflections, indicating that the bond of the conductive adhesive layers is sufficient, electric fields about 20% higher are needed to get there. Part of this difference is due to the lower mass of PZT present in the four-layer devices (i.e. while the total actuator thickness is approximately the same, the four-layer devices have four 60 μm PZT layers versus two 135 μm layers in the standard devices). Further, despite being nominally the same material, measurements of the dielectric constant of the 60 μm PZT show that it is about 80% (varying between 88% and 72% over the range of fields used in this study) of that of the 135 μm PZT at 120 Hz—figure 5(d) shows this comparison as a function of electric field and frequency. Putting these two effects together means that, at the same electric field (ξ), the input energy for the four-layer actuators (defined as $0.5 \times C \times V^2 = 0.5 \times \varepsilon_0 \times \varepsilon_r \times A \times d \times \xi^2$) is $(120/135) \times 0.8 \approx 71\%$ of that of the two-layer actuators. We can thus define an 'effective' electric field for the four-layer actuators that is about $0.71^{0.5} = 84\%$ of the actual field, but gives the same input energy as the two-layer actuators. Note that in our actual calculations, we use the entire measured dependency of dielectric constant on field. These plots are shown in figures 5(a)–(c), and show that the performance (i.e. the efficiency, defined as the mechanical output power

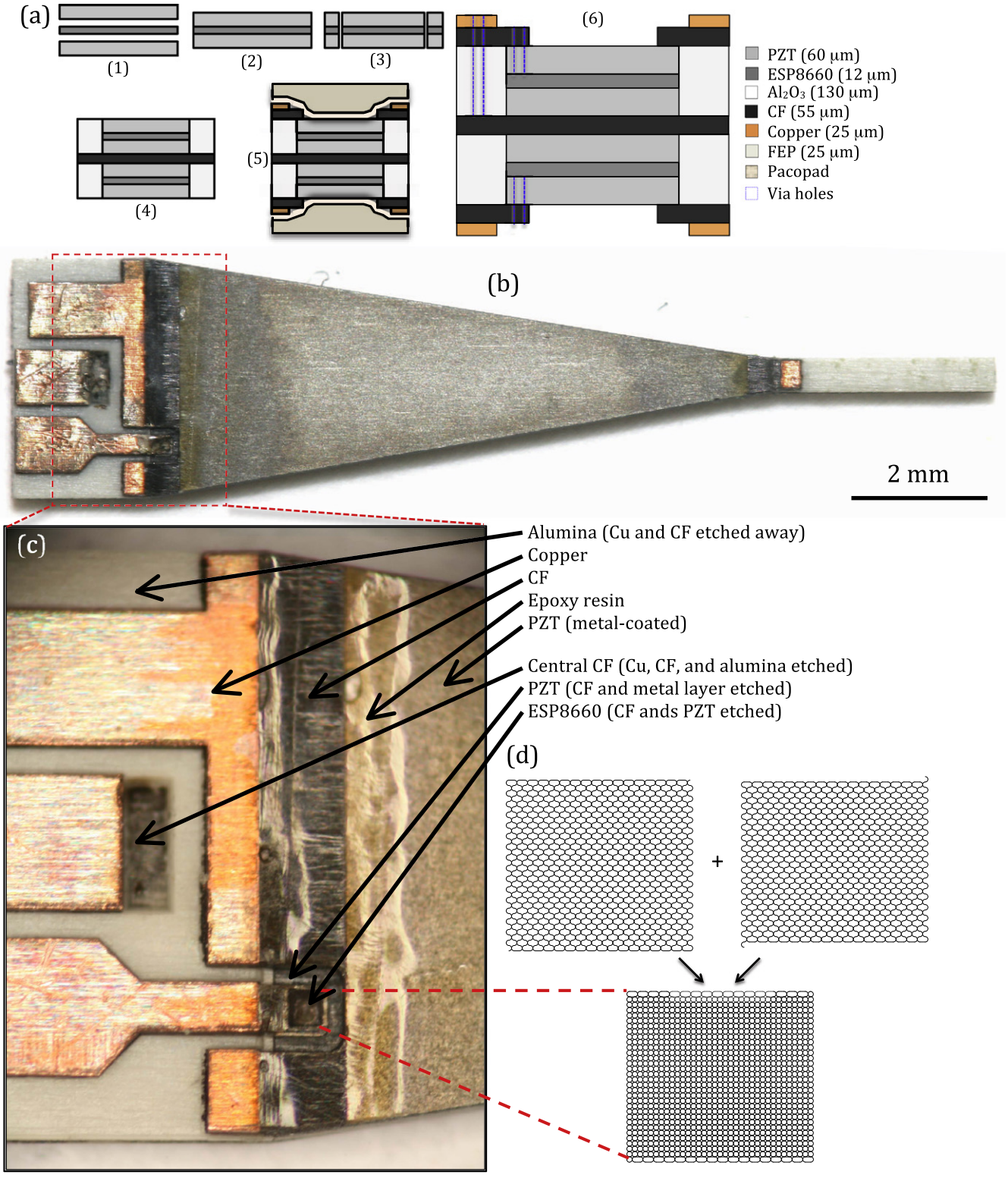

Figure 4. (a) Cross-section diagrams showing the fabrication process for the four-layer actuators. 1–2: Heat press bonds two 60 μm PZT sheets with a conductive adhesive film. 3: Bonded stack is laser-cut into rectangles. 4: These bonded stacks, along with alumina, are bonded to both sides of an uncured carbon fiber composite sheet in a heat press. 5: Copper and carbon fiber bridges are bonded around the pre-stack, using Pacopad and FEP to achieve more uniform pressure and form a smooth bond. 6: Via holes are etched to the appropriate layers for electrical contact. (b) Top-view optical image of the completed four-layer actuator. (c) Zoomed-in view of the actuator, showing etched holes for electrical contact and mechanical 'bridge' at the PZT–alumina interface. (d) 'Constant-curvature' raster pattern for uniform etching of the PZT.

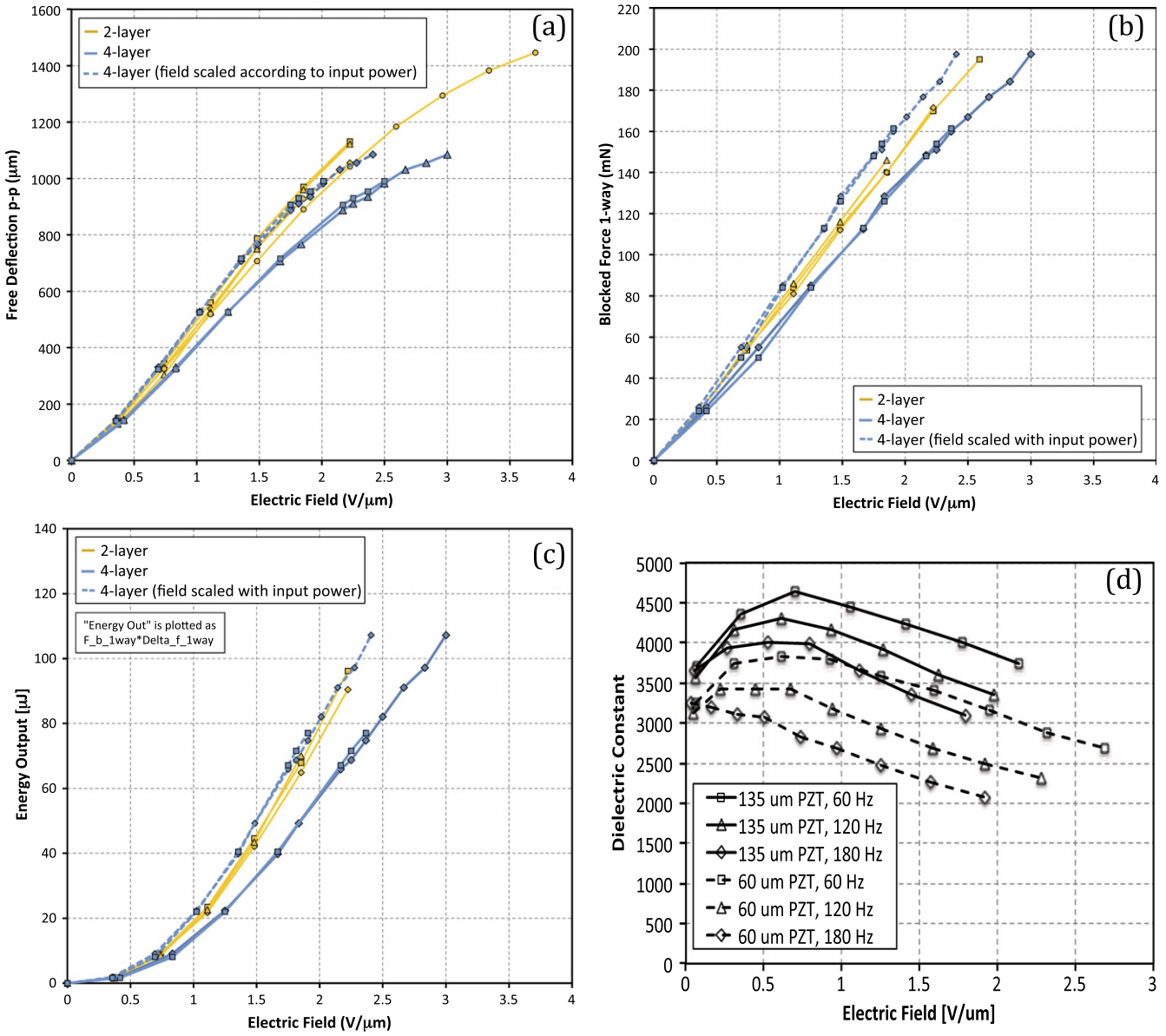

Figure 5. A performance comparison between two-layer and four-layer actuators for (a) free-deflection, (b) blocked-force, and (c) mechanical energy output. These are plotted versus electric field for both types of devices, and the four-layer actuators are also shown with the field rescaled to match the same input power. (d) A comparison of the dielectric constant of the 135 μm PZT and 60 μm PZT for various frequencies and electric fields (the nominal value is 3800).

divided by $0.5CV^2f$) of the four-layer actuators are up to 5% better than the two-layer ones. Confocal microscope images (figure 6) show that the microscopic grain structure differs as well—while the 135 μm PZT displays clear grain boundaries/faces, indicative of inter-granular fracture [1, 16], the 60 μm PZT images indicate that intra-granular fracture may be occurring instead. Further work is needed to determine any relations between these differences.

Finally, these results are used to plot p_r for fixed mechanical output power of the actual four-layer actuators (figure 7(a)), which are actually slightly better than the prediction, as well as the required actuator mass versus applied voltage for the actual four-layer actuators, and the corresponding battery mass based on the efficiency measurements/models discussed in section 2. As can be seen in figure 7(b), these results are very close (up to about 5% better) to the predicted 'ideal' four-layer actuator.

5. Discussion—scaling considerations

While the results presented so far demonstrate a clear benefit through power and overall mass reduction for the four-layer actuators as compared to the two-layer ones, this savings is due to the use of thinner material, so it is informative to consider the pros and cons of simply using the thinner material in a two-layer structure. For example, consider the shape changes that would be required to achieve the same free deflection and blocked force using thinner PZT (at the same electric field and the same strain): assuming that the thickness

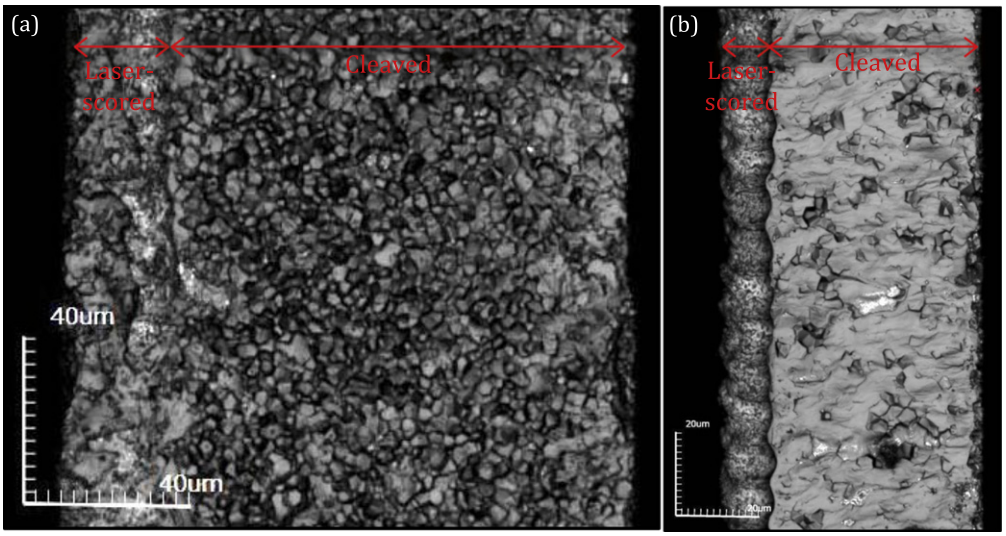

Figure 6. Confocal microscope images comparing the cleaved microstructure of (a) 135 μm PZT and (b) 60 μm PZT.

of the central CF layer is scaled with the PZT thickness, and the width ratio and length ratio are kept fixed, $\partial_f \propto L^2/t$ and $F_b \propto w\, t^2/L$ (where L, t, and w are the length, thickness, and width of the actuator, respectively). Thus, we would need to decrease L by a factor of $(t_{old}/t_{new})^{0.5}$ and increase w by a factor of $(t_{old}/t_{new})^{1.5}$. It can be seen that such scaling will eventually result in an actuator that is very wide and short, which could suffer from increased flexing perpendicular to the desired motion as well as being an unwieldy form factor for some applications. However, the two-layer process in significantly simpler, so the choice between the two should be made on a case-by case basis depending on the specific force and deflection requirements and space limitations. For example, the Harvard Robobee [14] uses actuators that are 9 mm long, 0.5 mm wide at the tip, and 1.75 mm wide at the base. Switching to 60 μm PZT would thus require an actuator 6 mm long, 1.7 mm wide at the tip, and 5.9 mm wide at the base—already as wide at the base as it is long, but a possibility depending on the space limitations. On the other hand, for a scaled-up version 'Bigbee' [17], the actuators are already as wide at the base as they are long (8.33 mm long, 0.5 mm tip, 8.6 mm base), so switching to 60 μm PZT would result in an extremely unwieldy actuator 5.6 mm long and 29 mm wide at the base. These examples suggest that, for a given device powered by a piezoelectric bimorph, multilayer actuators are attractive when scaling up, while scaling down points to two-layer actuators with thinner materials. More precisely, for a typical device with length scale £, the space available for actuator deflection is likely $\propto$ £, while the required mechanical energy might scale with $£^3$ (this is expected to be the case for powering flapping-wing vehicles, for example: if the wing-span is £, the operating frequency scales with $1/£$, the lift and drag forces scale with $£^2$, and the torque, and thus actuator energy, scales with $£^3$). In such a situation, the required actuator's length would scale with $£^{0.5}$ and its mean width would scale with $£^{2.5}$, clearly indicating that for larger size-scales either thicker PZT (requiring higher voltages) or more layers of PZT would be necessary to maintain a practical aspect ratio.

On the other hand, since scaling down could mitigate the need for multi-layer actuators, we demonstrate that our fabrication process is also capable of producing much smaller actuators using the standard two-layer method [1] but with 60 μm PZT and alumina (see appendix for further details). All of these actuators had a length of 2.65 mm (with 0.942 mm extension) and a 250 μm tip width—three different base widths were tested: 875 μm, 625 μm, and 375 μm. These actuators had weights of 1.74 mg, 1.36 mg, and 0.97 mg, respectively (recall that the 'standard' actuators described in [1] and the four-layer actuators in this paper were 9 mm long (with a 3.2 mm extension), 500 μm tip width, and 3.5 mm base width, and weighed ~45 mg). A cross-section indicating the material thicknesses for one of these actuators is shown in figure 8(a), while figure 8(b) shows a top view comparing these actuators with that used in the Robobee [14] (which is about half the width of the actuators described in the rest of this paper).

These downscaled PZT actuators are among the smallest PZT actuators fabricated using bulk materials, of similar size to those presented in [11]. Further, the bending curvatures of our actuators are about 4× higher than those in [11] at the same electric field (e.g. 9.5 m^{-1} versus 2.32 m^{-1} at 1.6 V μm^{-1}), despite being slightly thicker (160 μm versus 127 μm). The free deflection and blocked force results for these actuatorsare shown in figures 9(a) and (b), while energy density compared with that of the 'standard' and four-layer actuators is shown in figure 9(c). The energy densities are scaled by the gain factor terms to account for the different width ratios and length ratios (which affect the energy density). While the performance of these smaller actuators is 27% lower at the same electric field, recall that the input electrical energy scales with the dielectric constant, and is thus 12%–28% lower at the same field for the small actuators—hence, these actuators have 95% of the performance of the standard actuators when rescaled by input power and their physical

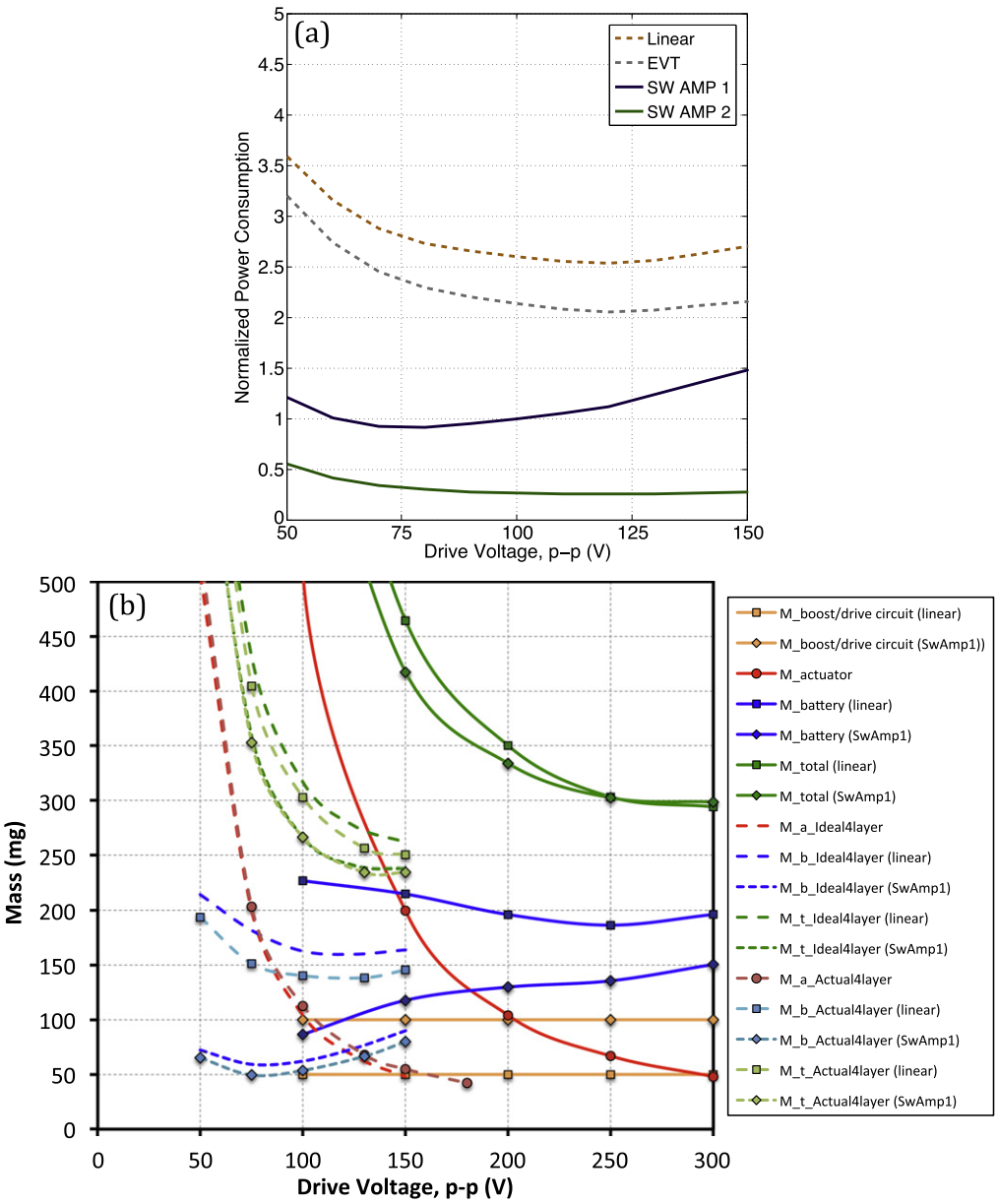

Figure 7. (a) The required power-supply power (normalized to $0.5CV^2f = 54$ mW) for constant mechanical output power ($d_{\text{f, 1-way}} \times F_{\text{b, 1-way}} \times f = 12.7$ mW) of the actuator (determined using the measurements from the actual four-layer actuators). (b) Required masses of an actuator, battery, boost-converter, and their total sum plotted versus voltage for a fixed output power of $d_{\text{f, 1-way}} \times F_{\text{b, 1-way}} \times f = 12.7$ mW. Solid lines are for two-layer actuators, while dashed lines are for four-layer actuators.

dimensions. Further, no significant variation ($<\pm 3\%$) in energy density was seen for the three widths tested, indicating that even at this scale we are not limited by any laser-induced damage zone.

6. Conclusions

In this work, we demonstrated a fabrication process for bulk PZT actuators consisting of four PZT plates with performance within a few percent of our two-layers actuators of the same size (for the same input energy), which reduces the power requirements by 24%–47% due to the higher efficiency of associated boost converter and drive circuitry at lower voltages. This allows these actuators to be used as drop-in replacements for any applications that previously used the two-layer actuators. Based on this power savings, we estimate an overall system weight (actuator, battery, and power electronics) savings of 15%–22%—for a vehicle such as the Harvard Robobee, this savings brings the goal of autonomous flight closer to reality.

Additionally, we showed that we could fabricate sub-mg two-layer actuators with energy densities ($d_{\text{f,1-way}} \times F_{\text{b,1-way}}/M$) of 1.4 μJ mg^{-1} (at an electric field of 2.25 V μm^{-1}), only a few percent less than that of the standard actuators [1] for the same input energy density ($0.5 \times C \times V^2/M = 5.3$ μJ mg^{-1}). These are among the smallest/lightest

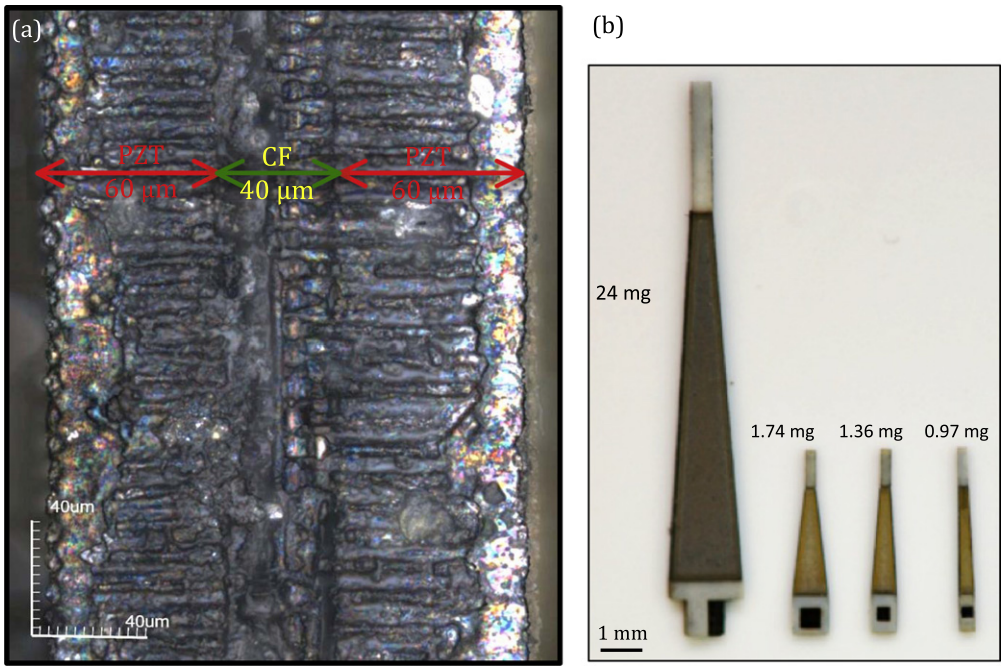

Figure 8. (a) Confocal microscope image of a cross-section of one of the sub-mg actuators. (b) Optical image of several of the small-scale actuators, along with an actuator of the size used in the Harvard Robobee for comparison. This image was taken before the addition of CF 'bridges' at the PZT–alumina boundaries.

piezoelectric actuators fabricated with bulk materials to date, and with such a high energy density.

Acknowledgments

The authors gratefully acknowledge support from the National Science Foundation (award # CMMI-1251729) and the Wyss Institute for Biologically Inspired Engineering at Harvard. Any opinions, findings, and conclusions or recommendations expressed in this material are those of the authors and do not necessarily reflect the views of the National Science Foundation.

Appendix

Fabrication details for mg-weight PZT actuators

In order to obtain sufficiently thin alumina for these actuators, 135 μm alumina is rastered down to 60 μm with a diode-pulsed solid-state laser (Photonics Industries DC150H-355, a Nd:YVO4 laser with 355 nm wavelength and 10 μm spot size), using a bi-directional cut setting, with 2 μm spacing, cutting with 0.63 W, at 10 cm s^{-1}, and 25 kHz, for six passes. This rastered alumina is cut into four rectangles using 0.63 W, at 15 cm s^{-1}, and 25 kHz, for 200 passes. The widths of the rectangles are 0.942 mm, which is the length of the actuator tip. Next, two rectangles with a 2.65 mm width (the length of the PZT part of the actuator) are cut out of the 60 μm PZT using 0.24 W, at 20 cm s^{-1}, and 20 kHz, for 300 passes. Lastly, a rectangle of 25 μm CF is cut out with 0.4 W, at 25 cm s^{-1}, 25 kHz, for 40 passes, with a 4.534 mm width to match the combined width of the PZT and two pieces of alumina.

The alumina and PZT pieces are then cleaned off with IPA. This is especially important for the alumina, in order to remove the particle remains from the rastering process, which affects the pieces' ability to adhere to the CF The actuators are stacked and built using the previously created method in [1] with a few variations, such as the pieces are aligned without pins and the 'bridge' supports at the base and tip of the actuators are glued on manually. Due to the fragility of the 60 μm PZT, x4 Gel-Film (a tacky film for temporary positioning; higher numbers correspond to greater adhesion, supplier: Delphon, Hayward, California, United States) is used in the layup instead of x8. It is best to have the non-rastered side of the alumina facing the CF, for better adhesion. To easily position the pieces for a close fit without breaking them, several drops of IPA are placed on the Gel-Film so that the pieces can be moved atop the liquid freely, and the alignments are made under a microscope. Once the IPA evaporates, the pieces stick to the Gel-Film, fixing them in place. The final stack is cured using the same heat press as in [1], at 50 psi.

Once cured, the release cuts to produce the individual actuators are made, following the rules described in [1], but with new settings. The cut through the alumina is made with 0.63 W, at 15 cm s^{-1}, and 25 kHz, for 200 passes. Next, the low power PZT cut is made with 0.24 W, at 20 cm s^{-1}, and 20 kHz, for 300 passes, which is followed by the high power PZT cut, made using 0.63 W, at 20 cm s^{-1}, and 20 kHz, for 10 passes. Finally, a square is rastered away from one of the alumina pieces at the base of actuator to reveal the CF to

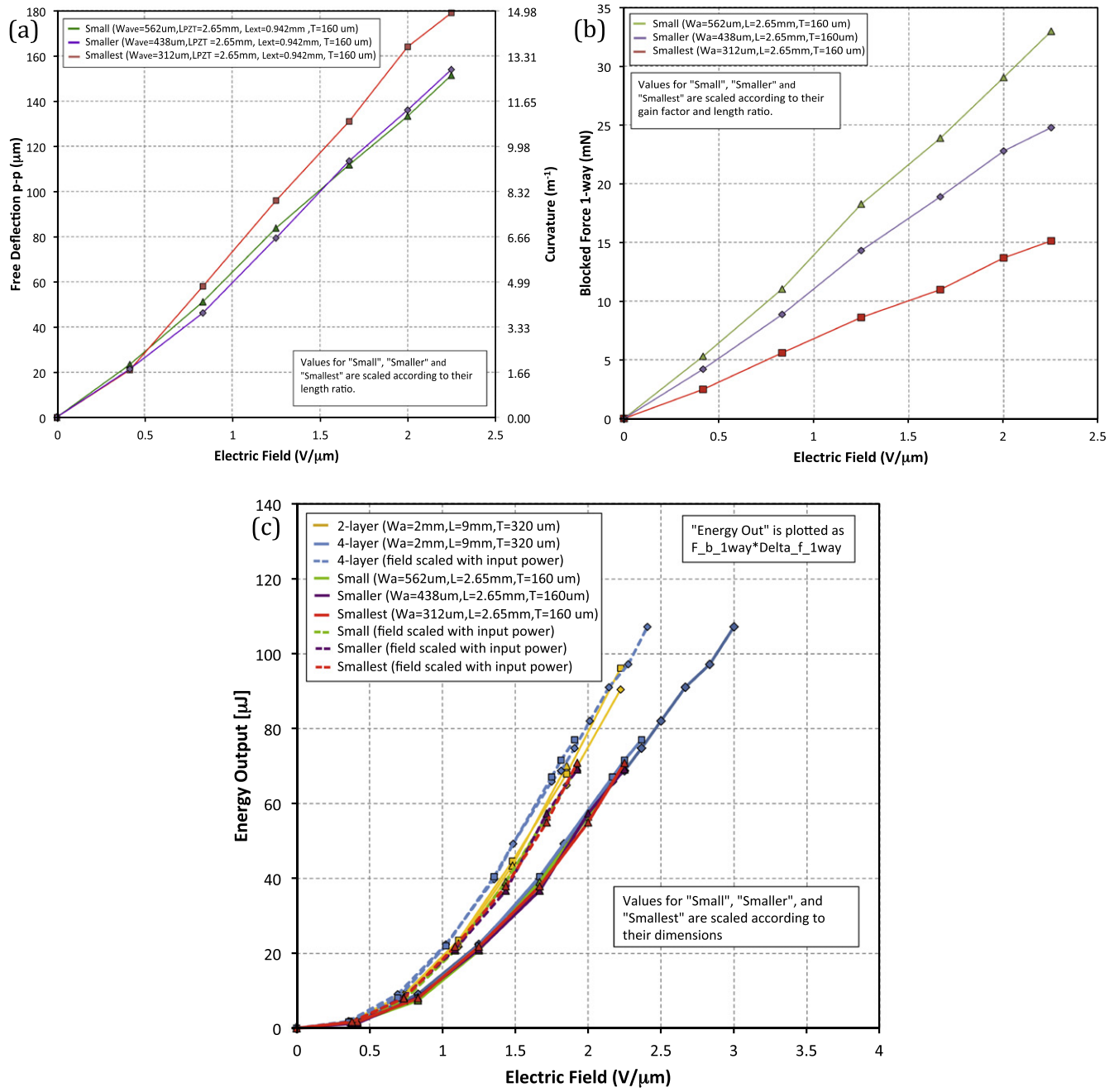

Figure 9. (a) Free-deflection and (b) blocked-force for three small actuators. All reported values for the are at the end of a 0.942 mm rigid extension; for some actuators, this extension was missing, in which case the measurements were rescaled accordingly. (c) The energy outputs of these three actuators are rescaled according to their dimensions and compared to that of the standard two-layer actuators and the new four-layer actuators.

make the electric connection. This rastering is done using the same bi-directional settings as earlier. In order not to cut or burn the CF, two passes are done at 70 kHz, two passes at 80 kHz, another four passes at 70 kHz, and a final two passes at 80 kHz.

To wire the actuators, 43 gauge wire is used, and the actuators need to be attached to an x8 Gel-Film, to avoid being blown away in the oven, while the epoxy cured. Finally, while coating the actuators in the parylene coater, the wires are sandwiched between x0 and x4 Gel-Film in order to hold the actuators in place.

References

[1] Jafferis N T, Smith M J and Wood R J 2015 Design and manufacturing rules for maximizing the performance of polycrystalline piezoelectric bending actuators *Smart Mater. Struct.* **24** 065023

[2] Hsu T-R 2008 *MEMS and Microsystems: Design, Manufacture, and Nanoscale Engineering* 2nd edn 576 (Hoboken, NJ: Wiley) ISBN: 978-0-470-08301-7

[3] Karpelson M, Wei G-Y and Wood R J 2012 Driving high voltage piezoelectric actuators in microrobotic applications *Sensors Actuators* A **176** 78–89

[4] Sano R, Inoue J-I, Kanda K, Fujita T and Maenaka K 2015 Fabrication of multilayer Pb (Zr, Ti) O3 thin film by sputtering deposition for MEMS actuator applications *Japan. J. Appl. Phys.* **54** 10ND03

[5] Kondo M, Hida M, Omote K, Taniguchi O, Mita T, Umemiya S and Kurihara K 2003 Preparation of $PbNi_{1/3}Nb_{2/3}O_3$–$PbTiO_3$–$PbZrO_3$ ceramic multilayer actuator with silver internal electrodes *Sensors Actuators* A **109** 143–8

[6] Izyumskaya N, Alivov Y-I, Cho S-J, Morkoç H, Lee H and Kang Y-S 2007 Processing, structure, properties, and applications of PZT thin films *Crit. Rev. Solid State Mater. Sci.* **32** 111–202

[7] Shen I Y (S), Cao G Z, Wu C-C and Lee C-G 2006 PZT thin-film meso- and micro devices *Ferroelectrics* **342** 15–34

[8] Aktakka E E, Peterson R L and Najafi K 2011 Multi-layer PZT stacking process for piezoelectric bimorph energy harvesters *11th Int. Conf. on Micro and Nanotechnology for Power Generation and Energy Conversion App. (PowerMEMS 11)* pp 139–42

[9] Yao K and Zhu W 1998 Improved preparation procedure and properties for a multilayer piezoelectric thick-film actuator *Sensors Actuators* A **71** 139–43

[10] Tran A T, Wunnicke O, Pandraud G, Nguyen M D, Schellevis H and Sarro P M 2013 Slender piezoelectric cantilevers of high quality AlN layers sputtered on Ti thin film for MEMS actuators *Sensors Actuators* A **202** 118–23

[11] Hareesh P, Misri I, Yang S and DeVoe D L 2012 Transverse interdigitated electrode actuation of homogeneous bulk PZT *J. Microelectromech. Syst.* **21** 1513–8

[12] Lok M, Zhang X, Helbling E F, Wood R J, Brooks D and Wei G Y 2015 A power electronics unit to drive piezoelectric actuators for flying microrobots *Custom Integrated Circuits Conf. (CICC)* pp 1–4

[13] Lok M, Brooks D, Wood R and Wei G Y 2013 Design and analysis of an integrated driver for piezoelectric actuators *Energy Conversion Congress and Exposition (ECCE)* pp 2684–91

[14] Ma K Y, Chirarattananon P, Fuller S B and Wood R J 2013 Controlled flight of a biologically inspired, insect-scale robot *Science* **340** 603–7

[15] Baisch A T and Wood R J 2009 Design and fabrication of the Harvard ambulatory micro-robot *14th Int. Symp. on Robotics Research* pp 715–30

[16] Guillon O, Thiebaud F, Perreux D, Courtois C, Champagne P and Crampon J 2005 New considerations about the fracture mode of PZT ceramics *J. Eur. Ceram. Soc.* **25** 2421–4

[17] Ma K Y, Chirarattananon P and Wood R J 2015 Design and fabrication of an insect-scale flying robot for control autonomy *2015 IEEE/RSJ Int. Conf. on Intelligent Robots and Systems (IROS)* pp 1558–64